BIOCHEMISTRY
including biophysical chemistry & molecular biology

Article

pubs.acs.org/biochemistry

A Theoretical Study of Phosphoryl Transfers of Tyrosyl-DNA Phosphodiesterase I (Tdp1) and the Possibility of a "Dead-End" Phosphohistidine Intermediate

Nathan J. DeYonker*,‡ and Charles Edwin Webster*,†,‡

†Department of Chemistry, Mississippi State University, Mississippi State, Mississippi 39762, United States

‡Department of Chemistry, The University of Memphis, 213 Smith Chemistry Building, Memphis, Tennessee 38152, United States

Supporting Information

ABSTRACT: Tyrosyl-DNA phosphodiesterase I (Tdp1) is a DNA repair enzyme conserved across eukaryotes that catalyzes the hydrolysis of the phosphodiester bond between the tyrosine residue of topoisomerase I and the 3′-phosphate of DNA. Atomic level details of the mechanism of Tdp1 are proposed and analyzed using a fully quantum mechanical, geometrically constrained model. The structural basis for the computational model is the vanadate-inhibited crystal structure of human Tdp1 (hTdp1, Protein Data Bank entry 1RFF). Density functional theory computations are used to acquire thermodynamic and kinetic data along the catalytic pathway, including the phosphoryl transfer and subsequent hydrolysis. Located transition states and intermediates along the reaction coordinate suggest an associative phosphoryl transfer mechanism with five-coordinate phosphorane intermediates. Similar to both theoretical and experimental results for phospholipase D, the proposed mechanism for hTdp1 also includes the thermodynamically favorable possibility of a four-coordinate phosphohistidine "dead-end" product.

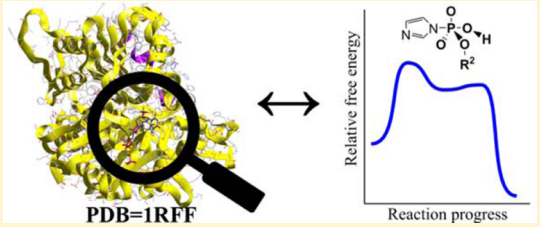

Phosphorus plays a crucial role in biochemistry, and phosphate esters (P-OR) are known leaving groups in hundreds of metabolic reactions in the bacterial, plant, and animal kingdoms.[1−5] The mechanism of P−OR bond breaking and bond forming is known as phosphoryl transfer, and the utilization of quantum chemistry techniques to study enzyme-catalyzed phosphoryl transfer has been a decades-long active subject of debate.[2,5−38] Proposed mechanisms for phosphoryl transfers generally fall into three categories: (1) fully "dissociative" mechanisms, in which a three-coordinate metaphosphate intermediate is formed, (2) fully "associative" mechanisms, in which a five-coordinate phosphorane intermediate is formed, or (3) concerted mechanisms without intermediates.

Tyrosyl-DNA phosphodiesterase I (Tdp1), a purported phospholipase D (PLD) superfamily member, is an enzyme known to participate in DNA repair mechanisms, as it catalyzes the hydrolysis of a phosphodiester bond between a tyrosine residue and a DNA 3′-phosphate moiety.[39−42] Tdp1 is suspected to have very high specificity, because there are only a few known occurrences of the required type of P−O bond in the eukaryotic cell.[43−46] Nevertheless, Tdp1 can be considered a 3-DNA end-processing enzyme, and its main function may be to hydrolyze the transient covalent bond formed between the active site tyrosine residue of DNA topoisomerase I (Top1) and 3′-phosphoryl DNA groups during DNA unwinding. Without properly functioning Tdp1 enzymes, the aforementioned covalent linkage can lead to single-strand or double-strand DNA breaks. Stalled Top1 enzymes caused by phenomena such as ionizing radiation or Top1 "poisons" (including anticancer medications such as camptothecin) can "collide" with the DNA replication fork, leading to cell death.[47−49] In fact, mutation of an active site histidine residue in human Tdp1 (hTdp1) has been implicated as a potential cause of the hereditary neurodegenerative disease spinocerebellar ataxia with axonal neuropathy (also called SCAN1).[50−54]

Our laboratory has conducted a series of computational studies of phosphoryl transfer enzymes, including β-phosphoglucomutase (β-PGM),[14,55] cyclic AMP-dependent protein kinase (cAPK),[19] and bacterial PLD.[21] In our study of *Streptomyces* sp. PMF PLD (or PLD_{PMF}), an ONIOM[56] QM:QM "cluster model"[14,55,57−63] was used on the basis of the X-ray crystal structure obtained by Leiros, McSweeney, and Hough[64,65] (PDB entry 1V0Y). On the basis of the various minima and transition states obtained, three "submechanisms" were proposed: (A) the first phosphoryl transfer and condensation of the model phospholipid headgroup, (B) the hydrolysis of the phosphohistidine intermediate, and (C) the *in vitro* second phosphoryl transfer leading to a "dead-end" four-coordinate phosphohistidine product. All three proposed submechanisms showed associative-type phosphoryl transfers with five-coordinate intermediates. A rationale for the short but observable lifetime of the five-coordinate intermediate akin to that observed in the PDB entry 1V0Y X-ray crystal structure

Received: April 14, 2015
Revised: June 2, 2015
Published: June 29, 2015

DOI: 10.1021/acs.biochem.5b00396
Biochemistry 2015, 54, 4236−4247

was given. Accordingly, computed relative free energies validated the dead-end four-coordinate phosphate intermediate as an extremely stable thermodynamic sink, akin to what is observed in the longer substrate-soaked and product-soaked X-ray crystal structures (PDB entries 1V0W, 1V0V, 1V0T, and 1V0U).[64] Examination of possible mechanisms of the enzyme on an atomic level with density functional theory (DFT) is driven by the intrinsic chemistry inferred by the X-ray crystal structures. Indeed, the "cluster model" has been successfully used to provide an exquisite level of mechanistic detail.[63]

Upon publication of the first sequencing and X-ray crystal structure of hTdp1 by Hol, Interthal, Champoux, and co-workers in 2001 and 2002,[66−68] they claimed that Tdp1 is a member of the PLD superfamily of enzymes.[68] This classification has propagated throughout the Tdp1 literature on structure, mutation, and pharmaceutical activity.[42,47,48,69−74] Interestingly, Tdp1 does not rigidly fit into the description of a PLD enzyme, other than its role in biology as a phosphodiesterase. For example, sequences of known Tdp1 enzymes do not contain the conserved $H_xK_{xxxx}D$ motif, but rather only conserve the H_xK part.[47,66,67,70,73,74] Though sequencing of Tdp1 is dissimilar to that of PLD, the Tdp1 active site still closely resembles that of PLD because of an asparagine residue occurring later in the sequence. Scheme 1 shows a two-dimensional (2D) cartoon of the native *Homo sapiens* Tdp1 active site (PDB entry 1JY1) and the bacterial PLD_{PMF} active site (PDB entry 1V0S).

Interestingly, the *pros* nitrogen atom of the C-terminal histidine (H263) of hTdp1 possesses a hydrogen bonding environment similar to that of the typical HKD motif of PLD_{PMF}, with a glutamate residue (E538) serving the same H-bond acceptor role that the PLD-conserved aspartate (D473) residue does.[66] Also similar is the R group of a nearby serine residue (S514 in hTdp1 and S463 in PLD_{PMF}) donating a hydrogen bond to the carboxylate group in E538. This extra H-bond stabilization of H263 (in hTdp1) and H170 (in PLD_{PMF}) may rationalize the formation of the covalent phosphohistidine bond on these histidines, rather than the active site histidine near the C-terminus (H493 in hTdp1 and H448 in PLD_{PMF}). Though the sequence homology of these two enzymes is fairly different, the general "construction" of the active sites is easily superposed (Scheme 1). The main difference between the two is the presence of Q294 in hTdp1 forming a hydrogen bond with H493 rather than an Asp or Glu residue. This fact likely alters the general acid−base chemistry of H493 with the phosphohistidine bond. There has been speculation in the literature that Tdp1, with its $H_xK_{(x)}N$ motif and wider differences in specificity upon comparison of prokaryotic and eukaryotic function, is less or divergently evolved compared to most members of the PLD superfamily and thus belongs in its own subclass of enzymes.[70,73,74]

Since the publication of the first X-ray crystal structures of hTdp1, a great deal of research has been conducted to generate inhibited and transition state/intermediate analogue crystal structures in attempts to better understand its function and substrate specificity. White, van Waardenburg, and co-authors have performed studies on Tdp1 to learn more about the relationship of this protein with the disease SCAN1, specifically mutation studies of the active site of yeast Tdp1 (yTdp1).[48,73,74] Their most recent study of yTdp1 contained a curious feature; after reanalyzing the data for the X-ray crystal structure (PDB entry 1Q32), they found that strong electron density near the *tele* nitrogen atom of the N-terminal histidine (H162) could be interpreted as a four-coordinate phosphohistidine similar in structure to the "dead-end" product observed in the *in vitro* PLD_{PMF} study.[21,64,73,74] After a period of substrate aging, the equilibrium can be driven toward a four-coordinate phosphate thermodynamic sink.

In this work, we will discuss comparisons between the phosphoryl transfer of human Tdp1 and PLD_{PMF} that are based on completely quantum mechanical models for Tdp1 and PLD. Kinetics and thermodynamics of a proposed phosphoryl transfer mechanism will be obtained using a model of tyrosyl-DNA phosphodiesterase I. The feasibility of substrate reorganization and formation of the dead-end phosphohistidine product will also be proposed.

Scheme 1

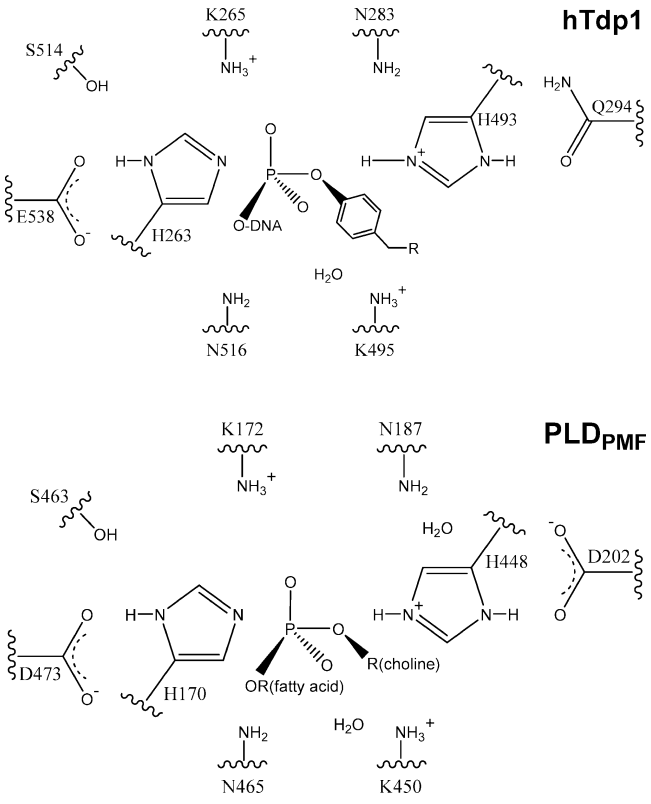

METHODS AND MODEL BUILDING

All computations were performed using the Gaussian09 software package.[75] For our quantum mechanical "cluster model", density functional theory (DFT) with the hybrid B3LYP functional was employed[76,77] with the 6-31G(d′) basis sets for N, O, and P atoms[78−80] and the 6-31G basis sets for C and H atoms. Structures containing vanadium atoms were computed with either the 6-31G(d) basis set on the V atom or the Hay and Wadt basis set as modified by Couty and Hall (V: 341/341/41), where the two outermost p functions have been replaced by a split of the optimized V 4p function and effective core potential (ECP) combination (LANL2DZ).[81,82] Free energy differences between all electron and ECP basis sets on the V atom were generally less than 0.8 kcal mol^{-1}. Thus, all discussion involving vanadium-centered substrates refers to computations using the modified Hay and Wadt basis set and LANL2DZ ECP. The default integration grids were used: the fine grid for two-electron integrals and gradients and the coarse

DOI: 10.1021/acs.biochem.5b00396
Biochemistry 2015, 54, 4236−4247

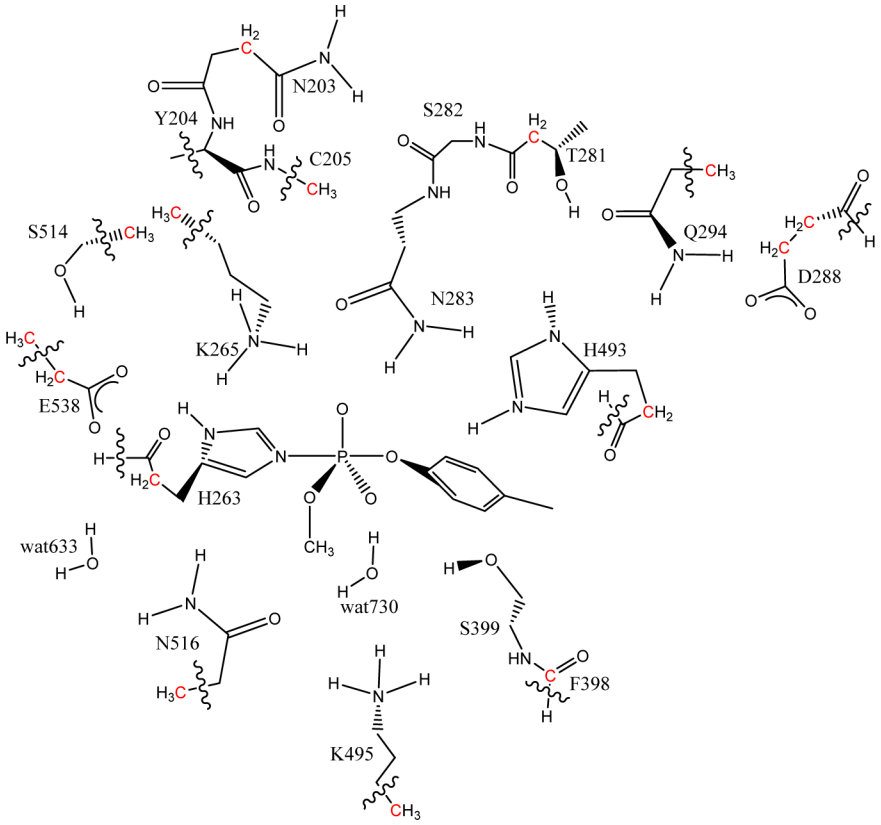

Figure 1. 2D structure of the hTdp1 "cluster model" based on PDB entry 1RFF. The 15 frozen carbon atoms are colored red.

grid for the Hessian. The gas-phase energies, gas-phase free energies, and solution-phase free energies of all reported structures are listed in Table S1 of the Supporting Information.

The structural basis for our computations was to begin with the geometry from the X-ray crystal structure of human Tdp1 in its intermediate analogue form complexed with vanadate, the octapeptide KLNYYDPR, and the tetranucleotide AGTT (PDB entry 1RFF).[70] Monoanionic substrates $[M(O)_2(OR^1)(OR^2)]^-$ are included, where M = P or V. In this work, "OR^1" will designate the substrate ligand involved in the first phosphoryl transfer and "OR^2" will designate the ligand involved in the second phosphoryl transfer. The octapeptide OR^1 ligand is trimmed to a *p*-cresolate ligand (called "OTyr" in this study), while the tetranucleotide (OR^2) is trimmed to a methoxy ligand (called "OMe" in this study). We are currently exploring rational design and construction of QM cluster active site models based on the topology of hydrogen bonding in geometries derived from X-ray crystal structures. This algorithm is currently based on modified versions of the *reduce*,[83] *probe*,[84] and *RINalyzer*[85,86] codes. Rather than inclusion of residues and solvent molecules based on a spherical/radial distance cutoff from an arbitrary point in the active site, the H-bond topology of the active site is exploited to create elliptical models. Combined with evidence that constrained backbone atoms in the QM cluster model can mimic the behavior of hydrophobic side chains in residues such as Ala and Ile, these rationally constructed active site models can minimize both the number of atomic constraints and the total number of atoms in the system, while also maximizing the percentage of included residues and fragments that are directly or indirectly participating in the proposed catalytic mechanism.[87]

Via this process, our cluster model contains 17 amino acid residues from the 1RFF X-ray crystal structure from chain A: N203, Y204, C205, H263, K265, T281, S282, N283, D288, Q294, F398, S399, H493, K495, S514, N516, and E538. Also, two explicit water molecules (denoted as wat633 from chain D and wat730 from chain A) are included in the active site model. Peripheral atoms on distant residues were truncated to reduce the size of the models and maintain neutral charge (see Table S2 of the Supporting Information for details). Figure 1 provides a 2D representation of the cluster model, including constrained atoms (in red).

X-ray crystal data for hTdp1 are generally recorded at pH 7.2−8.0, which suggests that all included Asp and Glu residues will be deprotonated, all Lys residues will be protonated, and all His residues will be neutral. However, deprotonation of either N in H493 is not consistent with the chemistry in the context of catalysis for a number of reasons. (1) If the *tele* nitrogen atom of H493 was deprotonated, then this residue would not be able to perform as a general acid in the experimentally proposed mechanism. (2) A proton bound to the *pros* nitrogen atom of H493 has favorable H-bond donation to both the backbone oxygen atom in T281 and the R group oxygen atom of Q294, both in our models and in the X-ray crystal structure. (3) A doubly protonated H493 creates a positively charged active site environment that would enhance the Coulombic attraction of the negatively charged phosphoryl group of the Top1 substrate. Overall, the cluster model has neutral charge when the substrate is included and contains 228 atoms in the proposed mechanism of the first phosphoryl transfer and 215 atoms after replacement of the cleaved *p*-cresolate ligand with a bulk solvent water molecule. Only 15 strategic atoms were needed to be constrained at their crystallographic positions to

DOI: 10.1021/acs.biochem.5b00396
Biochemistry 2015, 54, 4236−4247

Scheme 2

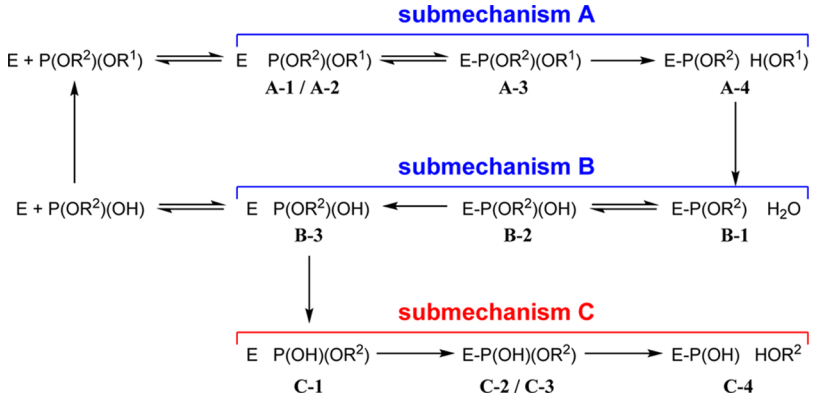

retain the general shape and H-bonding network of the active site. Typically, only the C^{α} atom of each major fragment was constrained. Exceptions were that (1) the C^{β} atoms for K265 and K495 were frozen, (2) the C^{γ} atom for N203 was frozen, and (3) the C^{α} and C^{β} atoms for D288 and the C^{β} and C^{γ} atoms for E538 were frozen.

All structures were geometry-optimized in the gas phase using standard gradient methods. The energy Hessian was evaluated at all stationary points to designate them as either minima or transition states at the computed level of theory. All reported minima have all real frequencies, and transition states have one imaginary frequency. Free energies are reported at 298.15 K and 1 atm and were determined using the computed, unscaled harmonic vibrational frequencies. Protein solvation energies were computed via single-point energy computations on the gas-phase equilibrium geometries using the COSMO polarizable conductor model (PCM) with UAKS sets of atomic radii, a nondefault electrostatic scaling factor of 1.2, and a dielectric constant (ε) of 4.0 to simulate the less polarized protein environment.

RESULTS AND DISCUSSION

Chemical Context of the Proposed Mechanism. The overall mechanism can be more easily described when broken down into three "submechanisms". A thorough description of thermodynamics, kinetics, and solution-phase energies of the submechanisms will be discussed separately in sections b–d. The first two submechanisms correspond to the *in vivo* catalytic cycle for the hydrolysis of Top1 to yield 3′-phosphate DNA and free tyrosine (Scheme 2, blue): the substrate–enzyme bonding and first phosphoryl transfer (section b) and subsequent hydrolysis event (section c). The third submechanism, postulated to occur *in vitro* (Scheme 2, red) is the second phosphoryl transfer (section d). These three submechanisms are separated by processes for which direct transition states will not be located computationally. Specifically, between the first phosphoryl transfer and hydrolysis, the cleaved "tyrosyl" (HOR^1, where R^1 = *p*-cresolate *in silico* and R^1 = a tyrosyl-containing polypeptide *in vivo* and/or *in vitro*) will exit the active site and be replaced by an incoming water molecule. In the hydrolysis and second phosphoryl transfer mechanisms, R^1 = H. Between the hydrolysis event and the second phosphoryl transfer, the equatorial OH and the axial OR^2 of the unbound substrate switch positions; that is, the substrate must be "reorganized". Mechanisms in this work are postulated in the context of the *in vitro* catalytic cycle. Thus, our discussion centers on the thermochemistry and kinetics of phosphoryl transfer and hydrolysis independent of substrate presentation and substrate specificity.

a. Beginning of the Catalytic Cycle of Human Tdp1. To properly model a conserved thermodynamic cycle for the three submechanisms, it is first necessary to model the native enzyme active site (i.e., without substrate). This "empty" active site will provide a reference energy for the catalytic cycle and is needed to determine the substrate binding energy. Migration of the substrate into the active site and displacement of water is an entropically favored process. Upon alignment of the backbone atoms of the hTdp1 vanadate-inhibited 1RFF X-ray crystal structure with the native human 1JY1 X-ray crystal structure, visual inspection shows two solvent water molecules with oxygen atom electron density near two of the equatorial oxygen atoms of the vanadate substrate. In the superposed structures, the distances between the solvent water oxygen atoms and the nearest equatorial oxygen atoms on the vanadate are 0.92 and 1.11 Å. With these two water molecules being "pushed" into the bulk solvent by an incoming substrate, we have chosen to model a "native" active site using the crystallographic positions of 1RFF. To model solvent position in similar X-ray crystal structures of hTdp1, the model substrate was replaced by two explicit water molecules, with heavy atoms placed in the relative coordinates of wat704 and wat918 in the 1JY1 structure (as well as the two explicit solvent molecules, wat633 and wat730, included in the general model). Our optimized native enzyme model is overlaid with the equivalently trimmed geometry from the 1JY1 X-ray crystal structure (Figure 2).

The root-mean-square deviation of the 15 carbons frozen at the crystallographic positions of 1RFF compared to the atomic positions of 1JY1 is only 0.175 Å. The two extra water molecules are in position to be H-bond donors to H263, and wat918 can also be an H-bond acceptor for the doubly protonated H493, which is the residue participating in the general acid catalysis of the substrate. Except for slight reorganization of the two lysine residues, there is no qualitative difference between the H-bonding network in the residues included within our native enzyme model and that of trimmed 1JY1. Relaxation of K265 and K495 occurs because of the missing bulk of the substrate. In our models that include substrate, the locations of these lysine residues match better with those in the 1RFF X-ray crystal structure.

b. Formation of the Initial Phosphohistidine Intermediate. In Scheme 2, a generalized depiction of the catalytic cycle of Tdp1 is presented. To guide the reader toward understanding the proposed *in silico* mechanism, a "plus" sign in the chemical formula designates enzyme and substrate at infinite separation.

DOI: 10.1021/acs.biochem.5b00396
Biochemistry 2015, 54, 4236–4247

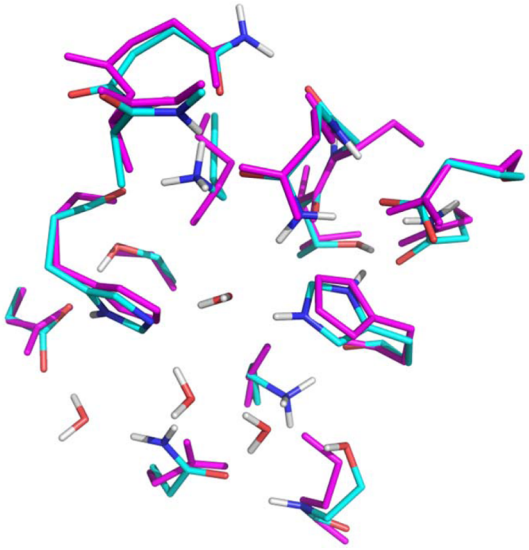

Figure 2. Overlay of the native geometry-optimized hTdp1 model (with 15 constrained carbons from the X-ray crystal structure of 1RFF) compared to the experimentally determined native hTdp1 X-ray crystal structure 1JY1 (magenta).

A space between the enzyme and substrate designates the typical "ES" enzyme–substrate species with the substrate in the active site but not covalently bonded to the enzyme. A dash between the enzyme and substrate designates the "EI" enzyme–phosphohistidine intermediate species.

At the beginning of the catalytic cycle, the $[P(O)_2(OR^2)(OR^1)]^-$ species enters the active site. Because of the method by which the enzyme active site and substrate have been truncated, there is no appropriate way to simulate or compute the diffusion kinetics of the substrate. However, the reaction energy and free energy of substrate binding from infinite separation to the active site can be reported. As expected, the gas-phase zero-point vibrational energy-corrected difference between the infinitely separated $[P(O)_2(OR^2)(OR^1)]^-$ and native enzyme with two extra waters versus displacement of those waters with the substrate is quite favorable, −62.5 kcal mol^{-1}. The gas-phase free energy (ΔG_{rxn} = −70.2 kcal mol^{-1}) of this reaction further favors the "product" side because of the displacement of two water molecules with one substrate molecule. When implicit solvent effects are included, the computed free energy of substrate binding (ΔG_{rxn} = −24.6 kcal mol^{-1}) becomes more reasonable.

With the $[P(O)_2(OR^2)(OR^1)]^-$ tetrahedral substrate situated in the active site, two minima relevant to the proposed mechanism were found. The Tdp1 active site is required to be quite large to accommodate the large $OR^{1/2}$ substituents ligands of the *in vivo* phosphodiester substrate. Therefore, it is not surprising that the truncated $[P(O)_2(OR^2)(OR^1)]^-$ substrate used in our model can occupy more than a single location in the active site region during its approach to the H263 residue. The initial enzyme–substrate complex, designated **A-1**, has the substrate located just outside of the active site pocket, with a distance of 4.53 Å between the substrate phosphorus and the attacking N atom of H263. For comparisons of relative free energies (gas phase and solution phase), the free energy of **A-1** will be the baseline (ΔG = 0.0 kcal mol^{-1}) of our free energy diagrams. To form the **A-2** structure, the OMe ligand of the substrate must undergo minor conformational change. However, attempts to find a transition state between the two unbound enzyme–substrate complexes (**A-TS-1-2**) were unsuccessful. This transition state is extremely unlikely to be the rate-limiting step of the entire enzyme mechanism. The **A-2** structure is aligned for the phosphohistidine nucleophilic addition to take place, with a P–N_{H263} bond distance of 3.023 Å. While in the gas phase, **A-1** and **A-2** are nearly isoergonic [$\Delta G_{(g)}$ of **A-2** = 0.7 kcal mol^{-1}], and the $\Delta\Delta G_{(soln)}$ of **A-1** and **A-2** is 7.2 kcal mol^{-1}. Interestingly, there are five hydrogen bonds between the enzyme and the substrate (including the wat730–substrate H-bond) in **A-2**, versus only three in **A-1**. The free energy penalty (exacerbated by the implicit solvation model) in **A-2** comes from repulsion of the ligand phosphorus negative charge with the unpaired electron on the H263 nitrogen atom. **A-2** leads to the transition state of P–N bond formation, **A-TS-2-3** with a $\Delta G^{\ddagger}_{(soln)}$ of 15.2 kcal mol^{-1}. In Schemes 3–10, the compact "cloud" schematic is

Scheme 3

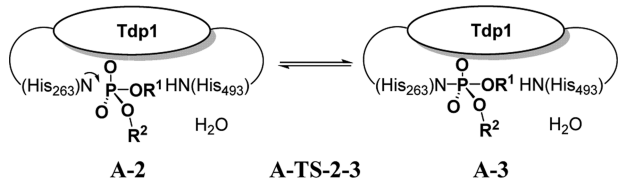

used. In this representation, only the substrate bond breaking/forming and general acid/base catalytic processes of the optimized structures are explicitly shown.

From nucleophilic attack of the substrate phosphorus by the *tele* N atom of H263, the five-coordinate phosphohistidine intermediate, **A-3**, is formed with a ΔG of 14.7 kcal mol^{-1}. While the **A-3** intermediate structure exists in a very short free energy well along the submechanism A reaction coordinate, the existence of **A-3** is indicative of a fully associative phosphoryl transfer mechanism. Via Hammond's postulate, **A-TS-2-3** is a very late transition state as the P–N bond distance contracts by only −0.13 Å to form **A-3**. Likewise, **A-TS-3-4** is an early transition state. At the five-coordinate intermediate, H493 is already poised to conduct the general acid catalysis of the P–O–Tyr substrate bond. The axial PO bond distance in **A-TS-3-4** increases by +0.33 Å, but as in **A-TS-2-3**, there is very little change in nuclear position throughout the enzyme model. Activation of the phosphohistidine intermediate occurs in **A-TS-3-4**, with a ΔG of 15.6 kcal mol^{-1}, and a $\Delta\Delta G$ of only 0.9 kcal mol^{-1} compared to that of **A-3**. Shown in Scheme 4, the

Scheme 4

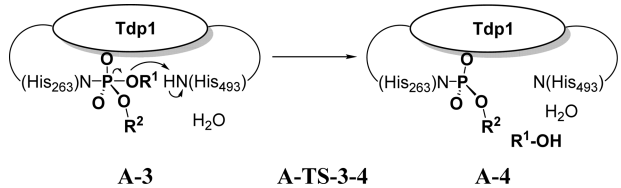

phosphoryl transfer is complete via a concerted condensation of the OR^1 ligand. The covalently bound pseudotetrahedral phosphohistidine intermediate (**A-4**) is slightly less stable than the **A-1** substrate–enzyme complex, with a ΔG of 3.5 kcal mol^{-1}. Submechanism A is complete, with the four-coordinate E-$P(O)_2(OR^2)$ complex and a free HOR^1 molecule.

DOI: 10.1021/acs.biochem.5b00396
Biochemistry 2015, 54, 4236–4247

c. Hydrolysis. Modeling the kinetics of diffusion, both the migration of the cleaved HOR^1 molecule (*p*-cresol *in silico*, the tyrosine-containing peptide *in vivo*) out of the active site and the migration of a bulk solvent water molecule into the active site, is outside of the scope and possibility for a time-independent QM cluster model. The relative free energies of this process can be computed, however. The **B-1** structure, with the same orientation of the pseudotetrahedral E-$P(O)_2(OR^2)$ complex and an explicit water molecule poised for hydrolysis, has a ΔG of 1.5 kcal mol^{-1}. This "reactant" for submechanism B also has a $\Delta\Delta G$ of −2.0 kcal mol^{-1} compared to "product" **A-4** in submechanism A. This thermoneutrality between HOR^1 and water also compares reasonably well to the difference in free energy between submechanisms A and B of PLD_{PMF} computed using the ONIOM QM:QM model ($\Delta\Delta G$ = +1.6 kcal mol^{-1}) . Scheme 5 depicts the activation of the incoming water molecule by H493 and the concerted addition of OH to the $P(O)_2(OR^2)$ substrate.

Scheme 5

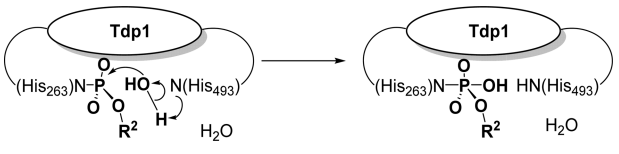

B-1 **B-TS-1-2** **B-2**

The transition state of hydrolysis, **B-TS-1-2**, has an overall ΔG of 7.8 kcal mol^{-1} or a $\Delta\Delta G^{\ddagger}$ of 6.3 kcal mol^{-1} to **B-1**. To our surprise, **B-2** has a rather long $P-N_{H263}$ bond length of 2.147 Å. The P−N bond distance in **B-2** is not substantially longer than the 2.092 Å $P-N_{H263}$ bond distance of **A-3**. However, the geometry of **B-2** is not-quite trigonal bipyramidal, which is somewhat odd, considering the intermediate lies in a deeper well than the five-coordinate intermediate computed in submechanism A, with a ΔG of 5.8 kcal mol^{-1} ($\Delta\Delta G$ = −2.0 compared to **B-TS-1-2**). The results are indicative of an associative mechanism for hydrolysis of hTdp1. The free energy of **B-2** relative to **B-TS-1-2** and **B-TS-2-3** is also lower than those of submechanisms A and B of our PLD_{PMF} ONIOM model, where those five-coordinate minima were effectively isoenergetic compared to their surrounding transition states.[21] The structure of **B-TS-2-3** closely resembles that of **B-2** but has an elongated P−N bond distance of 2.254 Å, which further distorts from the trigonal bipyramidal geometry. This very early transition state has an overall $\Delta G^{\ddagger}$ of 6.2 kcal mol^{-1} ($\Delta\Delta G$ = +0.4 kcal mol^{-1} compared to **B-2**). This transition state leads to **B-3** (Scheme 6), where the cleaved $P(O)_2(OR^2)$ substrate can then diffuse out of the active site, completing the catalytic cycle of DNA repair. Our computed structure for **B-3** has a ΔG of −2.4 kcal mol^{-1} relative to **A-1**. Like the overall proposed mechanism for PLD_{PMF}, the end of submechanism B has a free energy similar to that of the beginning of submechanism A.

Scheme 6

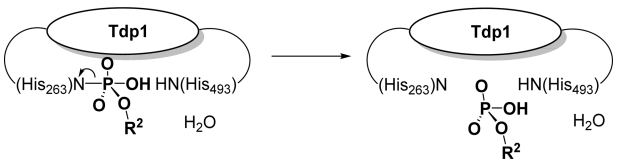

B-2 **B-TS-2-3** **B-3**

d. Dead-End Product. It was suggested by van Waardenburg and co-authors that yTdp1 could accordingly be rendered catalytically inactive after several catalytic cycles of DNA repair.[73,74] In their crystallization study, a four-coordinate phosphohistidine "dead-end" intermediate [presumably an E-$P(O)_3$ complex] was observed in the X-ray crystal structure of the yTdp1 H432R mutant (PDB entry 3SQ8). Similar behavior has been recognized in the PLD_{PMF} X-ray crystal structures, where Leiros and co-authors attributed the existence of the phosphate-bound product to "substrate aging" or substrate reorganization.[64] The results of our previous computations indicated that the catalysis of PLD_{PMF} can be short-circuited by substrate reorganization in the enzyme−hydrolyzed-substrate complex. Van Waardenburg and co-authors "speculate that the phosphate group originates from a similar *E. coli* phospholipid that is encountered by Tdp1 during expression. The more open active site of yTdp1 may allow processing of this substrate, whereas the tighter active site of hTdp1 may not." Indeed, there is very little difference in the primary sequences of yTdp1 and hTdp1 in their respective active sites. As will be shown below in submechanism C, if a phospholipid with a $P(O)_2(OR^2)(OH)$ structure can reorient itself within the active site of Tdp1, the thermodynamics and kinetics of the proposed mechanism are quite similar to those found with PLD_{PMF}. Does this imply that equilibrium can be driven toward the thermodynamic sink character of the E-$P(O)_3$ phosphate product for any member of the PLD superfamily given the appropriate artificial/*in vitro* conditions?

If the kinetic barrier of reorientation (Scheme 7) can be overcome within the active site, the "product" of reorientation

Scheme 7

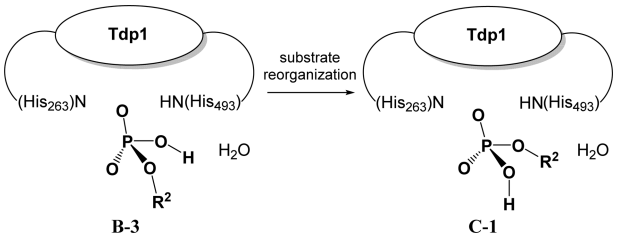

B-3 **C-1**

has a significantly lower free energy. Instead of migrating completely out of the active site, the $P(O)_2(OR^2)(OH)$ substrate (structure **B-3**) is positioned for another nucleophilic attack from the nitrogen atom in H263, but this time with the OR^2 group and OH group switched (**C-1**). In the theoretical study of PLD_{PMF}, an inversion of OR^2 and OH ligands in the five-coordinate phosphohistidine intermediate via turnstile rotation of the axial OH and equatorial OR^2 ligand in the enzyme-bound substrate had a free energy 2−7 kcal mol^{-1} higher than the free energy of activation for substrate reorganization. We have not recomputed this turnstile process for Tdp1. However, because of similarities in the models, it can be proposed that the stereomutation of the OH and OR^2 ligand will not be favorable energetically. In the PLD_{PMF} computations, we found the final structure of submechanism B to be nearly isoenergetic with the first structure of submechanism C ($\Delta\Delta G$ = 2.9 kcal mol^{-1}). In our Tdp1 model, **C-1** seems to be rather overstabilized as the $\Delta\Delta G$ of **C-1** compared to that of **B-3** is −13.6 kcal mol^{-1}. Initiation of a second phosphoryl transfer

DOI: 10.1021/acs.biochem.5b00396
Biochemistry 2015, 54, 4236−4247

occurs as the phosphorus−nitrogen bond of the substrate and H493 is re-formed in **C-TS-1-2** (Scheme 8). The free energy of activation for **C-TS-1-2** is 6.0 kcal mol^{-1}.

Scheme 8

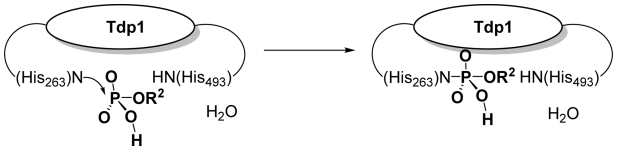

C-1 **C-TS-1-2** **C-2**

The five-coordinate phosphohistidine intermediate formed in structure **C-2** is effectively isoenergetic to **C-TS-1-2** in the solution phase, but has a gas-phase $\Delta\Delta G_{(g)}$ of −0.8 kcal mol^{-1}. A subtle conformational change in the orientation of wat730 brings about **C-TS-2-3**, which surprisingly has a free energy 1.4 kcal mol^{-1} higher than that of **C-TS-1-2**. While there is no obvious visual change in superposed **C-1** and **C-2**, the substrate−H263 P−N bond is shortened from 2.020 to 1.971 Å, and the axial P−O bond is lengthened from 1.818 to 1.878 Å. Both **C-2** and **C-3** are five-coordinate phosphohistidine intermediates with trigonal bipyramidal structures. This result suggests an associative phosphoryl transfer for hTdp1 submechanism C. The slight free energy penalty of **C-3** ($\Delta\Delta G$ = +0.7 kcal mol^{-1} compared to **C-2**) positions the axial POR^2 ligand for the second phosphoryl transfer occurring in **C-TS-3-4**. This very early transition state has a free energy only 0.2 kcal mol^{-1} higher than that of **C-3**.

At this point, a fascinating difference between the proposed submechanism C of Tdp1 and PLD$_{PMF}$ manifests itself. Unlike PLD$_{PMF}$, the appropriate proton on H493 is, at first, nucleophilic enough to transfer to the substrate OR^2 leaving group (Scheme 9). Proton transfer in the proposed mechanism

Scheme 9

C-3 **C-TS-3-4** **C-4**

of hTdp1 is different than submechanism C of PLD$_{PMF}$, where the leaving group scavenged the proton from the substrate hydroxyl group creating free methanol and an enzyme-bound P(O)$_3$ phosphate. The Tdp1 **C-4** structure has a free energy 11.6 kcal mol^{-1} lower than that of **C-TS-3-4**. There is a $\Delta\Delta G$ of +11.3 kcal mol^{-1} upon comparison of **C-4** to **C-1**, which is not representative of a thermodynamic sink. However, an essentially barrierless and concerted dual proton transfer (**C-TS-4-5**) donates the HOR^2 proton back to the H493 nitrogen atom while abstracting the proton from the substrate equatorial OH ligand (Scheme 10). The final **C-5** product has a ΔG of −14.0 kcal mol^{-1} relative to **A-1** and is presumably a "dead-end" product similar to that directly observed in studies of PLD$_{PMF}$.

In Figure 3, the solution-phase free energy diagram of the proposed mechanism is shown. Stoichiometrically balanced free energies of the total reaction mechanism are shown for the

Scheme 10

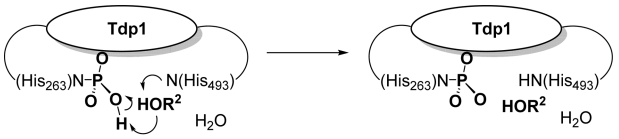

C-4 **C-TS-4-5** **C-5**

solution-phase computations of submechanisms A−C. In qualitative agreement with the proposed mechanism of PLD$_{PMF}$, the rate-limiting step of the *in vivo* catalytic cycle of hTdp1 is the first phosphoryl transfer in which general acid catalysis of the axial OR^1 ligand leads to HOR^1 loss and a bound four-coordinate P(O)$_2$(OR^2) substrate. The $\Delta G^{\ddagger}_{(soln)}$ of step **A-TS-3-4** is 15.6 kcal mol^{-1}. This can be compared to the free energy change of removing PO$_2$(OR$_2$)(OH) from the active site [from **B-3** to infinitely separated native enzyme model and PO$_2$(OR$_2$)(OH)$^-$], which is computed to be 23.3 kcal mol^{-1} for the Tdp1 model. This free energy of migration of the substrate from the active site can be used to approximate an upper limit to the free energy of activation required for substrate reorganization.[a] The free energy estimate for the Tdp1 model is 2.6 kcal mol^{-1} higher than the analogous value obtained in our investigation of PLD$_{PMF}$.

Using a QM cluster model of the hTdp1 active site, the results imply that substrate reorganization may be more difficult than was predicted in the QM model of the PLD$_{PMF}$ active site. However, speculation about differences in hTdp1 and PLD$_{PMF}$ kinetics cannot be conclusively made because of a variety of factors. The most important are steric and electrostatic differences in the OR^1 and OR^2 ligands of the *in vivo*/*in vitro* substrates that would be encountered by each enzyme. In the substrate pose encountered in submechanism A, the PLD$_{PMF}$ OR^1 group will be hydrophilic choline and the OR^2 group will be the long chain hydrophobic tail of the phospholipid. In the X-ray crystallographic experiment that generated the isolatable five-coordinate E-P(O)$_2$(OH)(OR^2) intermediate (PDB entry 1V0Y) and the dead-end product (PDB entries 1V0W, 1V0V, 1V0T, and 1V0U), there is not an extreme difference between the steric bulk of the choline headgroup and tail of their *in vitro* substrate (dibutyrylphosphatidyl choline, or diC4PC). The electrostatics of the OR^2 ligand is reversed in Tdp1. The single-strand DNA ligand occupying the OR^2 position of the substrate *in vivo* will possess robust negative charge along the chain, and there are quite a few hydrophilic residues in this narrow volume of the enzyme. From both PLD$_{PMF}$ and hTdp1 X-ray crystal structures, the OR^1 ligand is directed out of the active site cavity and toward the bulk solvent. For the "product" of submechanism B to convert to the "reactant" of submechanism C within the active site, the substrate must have room to reorganize, and reorganization is also required to be electrostatically favorable. Our computations suggest that, in agreement with the findings of van Waardenburg and co-workers,[73,74] the smaller active site cleft in hTdp1 may cause substrate reorganization to be far more kinetically disfavored compared to that of yTdp1 and PLD$_{PMF}$. However, it may be possible to isolate an X-ray crystal structure of dead-end phosphate-bound product or inhibited complex of hTdp1 given the appropriate *in vitro* conditions.

e. Thermodynamics of Vanadate Inhibition. For comparison to the 1RFF X-ray crystal structure, the five-coordinate intermediate has been reoptimized with a vanadium metal

DOI: 10.1021/acs.biochem.5b00396
Biochemistry 2015, 54, 4236−4247

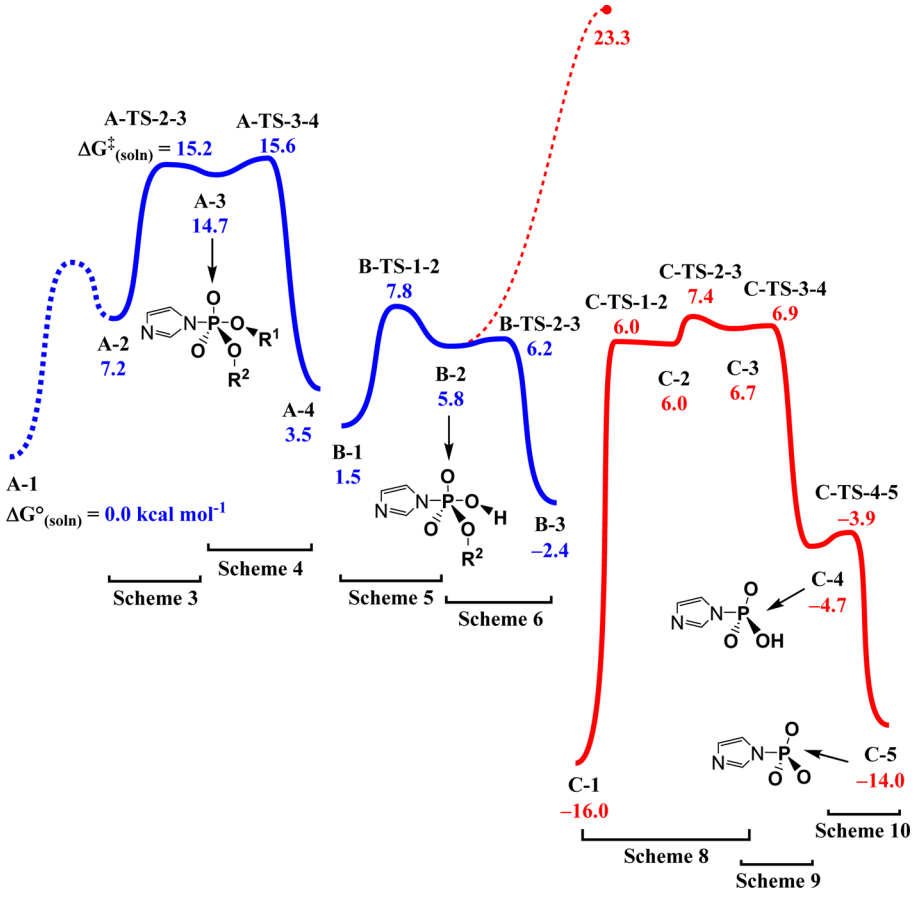

Figure 3. Free energy diagram of the proposed phosphoryl transfer mechanisms for hTdp1. Submechanisms A and B are shown with a blue curve, and the hypothesized submechanism C is shown with a red curve. As mentioned in the text, the transition state between **A-1** and **A-2** was not located, and the transition state energy is merely estimated via the dashed blue line. The red dashed line from **B-2** leads to the red dot, which marks the approximate relative energy of "substrate reorganization" from **B-3** to **C-1**.

center and OTyr and OMe ligands. A structure of free $[V(O)_2(OR^2)(OR^1)]^-$ has been optimized, along with structures analogous to those of four-coordinate **A-1** and five-coordinate **A-3** (which will be named **VA-1** and **VA-3**, respectively). No transition states between **VA-1** and **VA-3** were located. There is no corresponding **VA-2** structure analogous to that of **A-2** where the incoming substrate center is in line for nucleophilic attack by H263, likely because of the favorable binding of the $[V(O)_2(OR^2)(OR^1)]^-$ inhibitor.

A surprising result from computations with the V-centered complex is that the free energy difference between infinitely separated native enzyme/$[V(O)_2(OR^2)(OR^1)]^-$ and the E-$V(O)_2(OR^2)(OR^1)$ complex is smaller than that of $[P(O)_2(OR^2)(OR^1)]^-$. While ΔG_{rxn} = −24.6 kcal mol^{-1} for bringing $[P(O)_2(OR^2)(OR^1)]^-$ into the active site, the equivalent ΔG_{rxn} for the approach of $[V(O)_2(OR^2)(OR^1)]^-$ is −8.2 kcal mol^{-1}. The primary difference between the phosphorus-centered substrate and the vanadium-centered substrate is the relative energies of the five-coordinate intermediates. Whereas the P-centered complex (**A-3**) has a free energy 14.7 kcal mol^{-1} higher than that of **A-1** (and thus −9.8 kcal mol^{-1} lower than that of the infinitely separated enzyme and substrate), the five-coordinate vanadium-centered intermediate (**VA-3**) has a free energy lower than that of the **VA-1** complex [$\Delta\Delta G$ = −0.8 (Figure 4)]. These relative free energies provide quantitative validation of $[V(O)_2(OR^2)(OR^1)]^-$ as a thermodynamic inhibitor of the *in vitro* enzyme

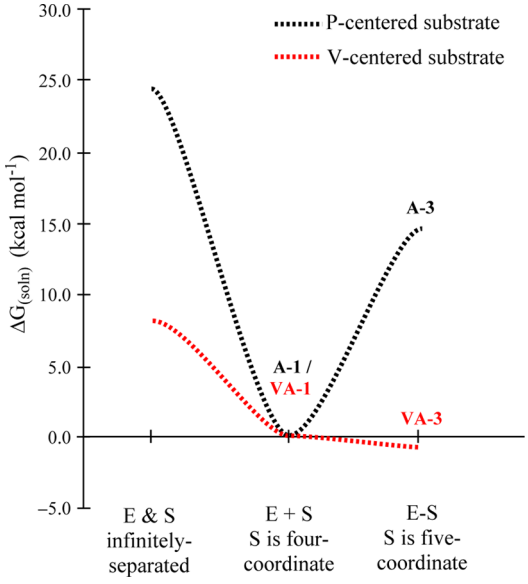

Figure 4. Relative free energies of optimized structures with phosphorus $[P(O)_2(OR^2)(OR^1)]^-$ and vanadium-centered $[V(O)_2(OR^2)(OR^1)]^-$ substrates along submechanism A.

mechanism. There is also excellent visual and structure agreement between the superposed **VA-3** structures and coordinates from the 1RFF X-ray crystal structure. For

DOI: 10.1021/acs.biochem.5b00396
Biochemistry 2015, 54, 4236−4247

example, the computed H263−vanadium equilibrium bond length is 2.138 Å, compared to a V−N bond distance of 2.144 Å in the X-ray crystal structure.

CONCLUSIONS

The *in vivo* catalytic activity of human Tdp1 (hTdp1) has been modeled with a QM-only active site cluster model containing 215−228 atoms depending on the substrate. The substrate has been modeled with $[P(O)_2(OR^2)(OR^1)]^-$, where the *in vivo* octapeptide OR^1 ligand is trimmed to a *p*-cresolate ligand (called "OTyr" in this study), and the tetranucleotide (OR^2) ligand is trimmed to methoxy (called "OMe" in this study). The proposed submechanisms outlined here are quite similar to those given in our computational study of PLD_{PMF}.

In submechanism A, the substrate has migrated into the active site, which is exergonic by 24.6 kcal mol^{-1}. Nucleophilic attack of the phosphorus atom by the appropriate N atom on H263 occurs, and a five-coordinate phosphohistidine intermediate is formed. The existence of this stationary point along the reaction allows an associative phosphoryl transfer mechanism to be proposed. A concerted condensation and ejection of the OR^1 leaving group occurs, forming HOR^1. This transition state (**A-TS-3-4**) is the overall rate-limiting step of the enzyme mechanism, with a $\Delta G^{\ddagger}$ of 15.6 kcal mol^{-1} compared to the initial enzyme−substrate complex (**A-1**). At the end of submechanism A, the covalently bound pseudotetrahedral phosphohistidine intermediate remains, while the free HOR^1 alcohol migrates out of the active site and is replaced by a water molecule from the bulk solvent. In submechanism B, hydrolysis of the four-coordinate substrate occurs. In the proposed submechanism B, a five-coordinate trigonal bipyramidal E-$P(O)_2(OR^2)(OH)$ minimum exhibits a quite long P−N interaction but still proceeds through an associative mechanism.

On the basis of the results from this study of hTdp1, an *in vitro* "dead-end" product can be observed, similar to the results from PLD_{PMF}. While submechanism C is shown to be thermodynamically favorable, steric and electronic effects from residues on the periphery of the active site may cause hTdp1 to be less promiscuous than PLD_{PMF} and yeast Tdp1. This second phosphoryl transfer also goes through a five-coordinate phosphohistidine intermediate and thus is proposed to undergo an associative mechanism. Computationally, it is suggested that the free energy of activation for substrate reorganization is ∼2.5 kcal mol^{-1} higher for hTdp1 than for PLD_{PMF}. This kinetic deterrence provides evidence that the hTdp1 active site might not be as amenable to being pushed toward a dead-end phosphate product. The five-coordinate vanadate intermediate has a free energy slightly lower than that of the infinitely separated substrate/enzyme, as well as the noncovalently bound enzyme−substrate intermediate, consistent with the experimental observation of a vanadate-inhibited structure.

Recently, van Waardenburg and co-workers reported that when H182 (yTdp1) is replaced with a small chain residue, the neighboring conserved histidine residue (yTdp1 H181) can act as an alternative nucleophile in forming the phosphohistidine intermediate (although the catalytic activity is considerably lower).[88] In hTdp1, this neighboring residue is H262, which is not included in the currently reported QM cluster model. The exploration of Tdp1 in the context of SCAN1 therapy and active site mutations with larger models (QM and layered QM/MM models) are planned for future studies.

Though the active site structure of hTdp1 does not mirror the typical HKD motif of the PLD superfamily, there is significant overlap in overall structure and function. It may be more difficult to drive *in vitro* equilibrium conditions toward a dead-end four-coordinate phosphate bound to hTdp1, but we encourage efforts to crystallize and characterize product complexes of Tdp1 with the same properties as those observed in PLD_{PMF}. From the point of view of atom level thermodynamics and kinetics, we have presented a QM cluster model that validates experimental findings and reveals interesting new questions about the relationships between members of the PLD superfamily.

ASSOCIATED CONTENT

Supporting Information

A table containing total and relative energies of each species, information about model creation and trimming of residues, and Cartesian coordinates of discussed structures. The Supporting Information is available free of charge on the ACS Publications website at DOI: 10.1021/acs.biochem.5b00396.

AUTHOR INFORMATION

Corresponding Authors

*E-mail: ewebster@chemistry.msstate.edu.
*E-mail: ndyonker@memphis.edu.

Funding

The National Science Foundation (CAREER Grant CHE 0955723), Mississippi State University, and the University of Memphis Department of Chemistry, the University of Memphis High Performance Computing Facility, and Computational Research on Materials Institute (CROMIUM) are gratefully acknowledged for funding this work.

Notes

The authors declare no competing financial interest.

ABBREVIATIONS

DFT, density functional theory; QM, quantum mechanical; ECP, effective core potential; PLD, phospholipase D; Tdp1, tyrosyl-DNA phosphodiesterase I; hTdp1, human tyrosyl-DNA phosphodiesterase I; yTdp1, yeast tyrosyl-DNA phosphodiesterase I; Top1, DNA topoisomerase I; SCAN1, spinocerebellar ataxia with axonal neuropathy; PDB, Protein Data Bank.

ADDITIONAL NOTE

[a]Explicitly determining the free energy of activation for the diffusional process is complicated by a gradient in substrate−solvent interactions from the protein environment to the bulk solvent, as well as possible limitations in our computational model. Thus, this value of 23.3 kcal mol^{-1} also approximates an upper limit of free energy of activation for the diffusional process.

REFERENCES

(1) Allen, K. N., and Dunaway-Mariano, D. (2004) Phosphoryl group transfer: Evolution of a catalytic scaffold. *Trends Biochem. Sci. 29*, 495−503.

(2) Benkovic, S. J., and Schray, K. J. (1978) The Mechanism of Phosphoryl Transfer. In *Transition States of Biochemical Processes* (Gandour, R. D., and Schowen, R. L., Eds.) pp 493−527, Plenum Press, New York.

(3) Cleland, W. W., and Hengge, A. C. (1995) Mechanisms of phosphoryl and acyl transfer. *FASEB J. 9*, 1585−1594.

DOI: 10.1021/acs.biochem.5b00396
Biochemistry 2015, 54, 4236−4247

(4) Holmes, R. R. (2004) Phosphoryl transfer enzymes and hypervalent phosphorus chemistry. *Acc. Chem. Res. 37*, 746−753.
(5) Knowles, J. R. (1980) Enzyme-Catalyzed Phosphoryl Transfer-Reactions. *Annu. Rev. Biochem. 49*, 877−919.
(6) Marcos, E., Crehuet, R., and Anglada, J. M. (2008) Inductive and external electric field effects in pentacoordinated phosphorus compounds. *J. Chem. Theory Comput. 4*, 49−63.
(7) Mercero, J. M., Barrett, P., Lam, C. W., Fowler, J. E., Ugalde, J. M., and Pedersen, L. G. (2000) Quantum mechanical calculations on phosphate hydrolysis reactions. *J. Comput. Chem. 21*, 43−51.
(8) Orth, E. S., Brandão, T. A. S., Souza, B. S., Pliego, J. R., Vaz, B. G., Eberlin, M. N., Kirby, A. J., and Nome, F. (2010) Intramolecular Catalysis of Phosphodiester Hydrolysis by Two Imidazoles. *J. Am. Chem. Soc. 132*, 8513−8523.
(9) Re, S. Y., Imai, T., Jung, J., Ten-No, S., and Sugita, Y. (2011) Geometrically Associative Yet Electronically Dissociative Character in the Transition State of Enzymatic Reversible Phosphorylation. *J. Comput. Chem. 32*, 260−270.
(10) Swamy, K. C. K., and Kumar, N. S. (2006) New features in pentacoordinate phosphorus chemistry. *Acc. Chem. Res. 39*, 324−333.
(11) Wilkie, J., and Gani, D. (1996) Comparison of inline and non-inline associative and dissociative reaction pathways for model reactions of phosphate monoester hydrolysis. *J. Chem. Soc., Perkin Trans. 2*, 783−787.
(12) Fersht, A. (1999) *Structure and Mechanism in Protein Science: A Guide to Enzyme Catalysis and Protein Folding*, W. H. Freeman and Co., New York.
(13) Lahiri, S. D., Zhang, G. F., Dunaway-Mariano, D., and Allen, K. N. (2003) The pentacovalent phosphorus intermediate of a phosphoryl transfer reaction. *Science 299*, 2067−2071.
(14) Webster, C. E. (2004) High-energy intermediate or stable transition state analogue: Theoretical perspective of the active site and mechanism of β-phosphoglucomutase. *J. Am. Chem. Soc. 126*, 6840−6841.
(15) Tremblay, L. W., Zhang, G. F., Dai, J. Y., Dunaway-Mariano, D., and Allen, K. N. (2005) Chemical confirmation of a pentavalent phosphorane in complex with β-phosphoglucomutase. *J. Am. Chem. Soc. 127*, 5298−5299.
(16) Baxter, N. J., Blackburn, G. M., Marston, J. P., Hounslow, A. M., Cliff, M. J., Bermel, W., Williams, N. H., Hollfelder, F., Wemmer, D. E., and Waltho, J. P. (2008) Anionic charge is prioritized over geometry in aluminum and magnesium fluoride transition state analogs of phosphoryl transfer enzymes. *J. Am. Chem. Soc. 130*, 3952−3958.
(17) Baxter, N. J., Olguin, L. F., Golicnik, M., Feng, G., Hounslow, A. M., Bermel, W., Blackburn, G. M., Hollfelder, F., Waltho, J. P., and Williams, N. H. (2006) A Trojan horse transition state analogue generated by MgF_3^- formation in an enzyme active site. *Proc. Natl. Acad. Sci. U.S.A. 103*, 14732−14737.
(18) Marcos, E., Field, M. J., and Crehuet, R. (2010) Pentacoordinated phosphorus revisited by high-level QM/MM calculations. *Proteins: Struct., Funct., Bioinf. 78*, 2405−2411.
(19) Leigh, K. N., and Webster, C. E. (2014) Theoretical studies of cyclic adenosine monophosphate dependent protein kinase: Native enzyme and ground-state and transition-state analogues. *Dalton Trans. 43*, 3039−3043.
(20) Griffin, J. L., Bowler, M. W., Baxter, N. J., Leigh, K. N., Dannatt, H. R. W., Hounslow, A. M., Blackburn, G. M., Webster, C. E., Cliff, M. J., and Waltho, J. P. (2012) Near attack conformers dominate β-phosphoglucomutase complexes where geometry and charge distribution reflect those of substrate. *Proc. Natl. Acad. Sci. U.S.A. 109*, 6910−6915.
(21) DeYonker, N. J., and Webster, C. E. (2013) Phosphoryl Transfers of the Phospholipase D Superfamily: A Quantum Mechanical Theoretical Study. *J. Am. Chem. Soc. 135*, 13764−13774.
(22) Andrews, L. D., Fenn, T. D., and Herschlag, D. (2013) Ground State Destabilization by Anionic Nucleophiles Contributes to the Activity of Phosphoryl Transfer Enzymes. *PLoS Biol. 11*, e1001599.
(23) Baker, D. L., Pham, T. C. T., and Sparks, M. A. (2013) Structure and catalytic function of sphingosine kinases: Analysis by site-directed mutagenesis and enzyme kinetics. *Biochim. Biophys. Acta 1831*, 139−146.
(24) Chen, S.-L., and Liao, R.-Z. (2014) Phosphate Monoester Hydrolysis by Trinuclear Alkaline Phosphatase; DFT Study of Transition States and Reaction Mechanism. *ChemPhysChem 15*, 2321−2330.
(25) Das, U., Wang, L. K., Smith, P., Jacewicz, A., and Shuman, S. (2014) Structures of bacterial polynucleotide kinase in a Michaelis complex with GTP·Mg^{2+} and 5′-OH oligonucleotide and a product complex with GDP·Mg^{2+} and 5′-PO_4 oligonucleotide reveal a mechanism of general acid-base catalysis and the determinants of phosphoacceptor recognition. *Nucleic Acids Res. 42*, 1152−1161.
(26) Elsaesser, B., Fels, G., and Weare, J. H. (2014) QM/MM Simulation (B3LYP) of the RNase A Cleavage-Transesterification Reaction Supports a Triester A(N) + D-N Associative Mechanism with an O2′H Internal Proton Transfer. *J. Am. Chem. Soc. 136*, 927−936.
(27) Gerlits, O., Das, A., Keshwani, M. M., Taylor, S., Waltman, M. J., Langan, P., Heller, W. T., and Kovalevsky, A. (2014) Metal-Free cAMP-Dependent Protein Kinase Can Catalyze Phosphoryl Transfer. *Biochemistry 53*, 3179−3186.
(28) Gu, H., Zhang, S., Wong, K.-Y., Radak, B. K., Dissanayake, T., Kellerman, D. L., Dai, Q., Miyagi, M., Anderson, V. E., York, D. M., Piccirilli, J. A., and Harris, M. E. (2013) Experimental and computational analysis of the transition state for ribonuclease A-catalyzed RNA 2′-O-transphosphorylation. *Proc. Natl. Acad. Sci. U.S.A. 110*, 13002−13007.
(29) Heldenbrand, H., Janowski, P. A., Giambasu, G., Giese, T. J., Wedekind, J. E., and York, D. M. (2014) Evidence for the Role of Active Site Residues in the Hairpin Ribozyme from Molecular Simulations along the Reaction Path. *J. Am. Chem. Soc. 136*, 7789−7792.
(30) Jin, Y., Bhattasali, D., Pellegrini, E., Forget, S. M., Baxter, N. J., Cliff, M. J., Bowler, M. W., Jakeman, D. L., Blackburn, G. M., and Waltho, J. P. (2014) α-Fluorophosphonates reveal how a phosphomutase conserves transition state conformation over hexose recognition in its two-step reaction. *Proc. Natl. Acad. Sci. U.S.A. 111*, 12384−12389.
(31) Kellerman, D. L., York, D. M., Piccirilli, J. A., and Harris, M. E. (2014) Altered (transition) states: Mechanisms of solution and enzyme catalyzed RNA 2′-O-transphosphorylation. *Curr. Opin. Chem. Biol. 21*, 96−102.
(32) Kellett, W. F., and Richards, N. G. J. (2014) Phosphoryl Transfer Transition State Computationally Modeled by MgF_3^- in the Oncogenetically Indicated GTPase Protein RhoA and its Activating Protein RhoA·GAP. *Biophys. J. 106*, 807A.
(33) Lee, Y., Villar, M. T., Artigues, A., and Beamer, L. J. (2014) Promotion of Enzyme Flexibility by Dephosphorylation and Coupling to the Catalytic Mechanism of a Phosphohexomutase. *J. Biol. Chem. 289*, 4674−4682.
(34) Medeiros, M., Wanderlind, E. H., Mora, J. R., Moreira, R., Kirby, A. J., and Nome, F. (2013) Major mechanistic differences between the reactions of hydroxylamine with phosphate di- and tri-esters. *Org. Biomol. Chem. 11*, 6272−6284.
(35) Rahimian, M., Yeole, S. D., and Gejji, S. P. (2014) Mechanistic insights for β-cyclodextrin catalyzed phosphodiester hydrolysis. *J. Mol. Model. 20*, 2198.
(36) Rudbeck, M. E., Blomberg, M. R. A., and Barth, A. (2013) Hydrolysis of the E2P Phosphoenzyme of the Ca^{2+}-ATPase: A Theoretical Study. *J. Phys. Chem. B 117*, 9224−9232.
(37) Whittier, S. K., Hengge, A. C., and Loria, J. P. (2013) Conformational Motions Regulate Phosphoryl Transfer in Related Protein Tyrosine Phosphatases. *Science 341*, 899−903.
(38) Wiersma-Koch, H., Sunden, F., and Herschlag, D. (2013) Site-Directed Mutagenesis Maps Interactions That Enhance Cognate and Limit Promiscuous Catalysis by an Alkaline Phosphatase Superfamily Phosphodiesterase. *Biochemistry 52*, 9167−9176.
(39) Yang, S. W., Burgin, A. B., Huizenga, B. N., Robertson, C. A., Yao, K. C., and Nash, H. A. (1996) A eukaryotic enzyme that can

DOI: 10.1021/acs.biochem.5b00396
Biochemistry 2015, 54, 4236−4247

disjoin dead-end covalent complexes between DNA and type I topoisomerases. *Proc. Natl. Acad. Sci. U.S.A. 93*, 11534−11539.
(40) Inamdar, K. V., Pouliot, J. J., Zhou, T., Lees-Miller, S. P., Rasouli-Nia, A., and Povirk, L. F. (2002) Conversion of phosphoglycolate to phosphate termini on 3′ overhangs of DNA double strand breaks by the human tyrosyl-DNA phosphodiesterase hTdp1. *J. Biol. Chem. 277*, 27162−27168.
(41) Pouliot, J. J., Yao, K. C., Robertson, C. A., and Nash, H. A. (1999) Yeast gene for a Tyr-DNA phosphodiesterase that repairs topoisomerase I complexes. *Science 286*, 552−555.
(42) Raymond, A. C., and Burgin, A. B. (2006) Tyrosyl-DNA phosphodiesterase (Tdp1) (3′-phosphotyrosyl DNA phosphodiesterase). *DNA Repair 409* (Part B), 511−524.
(43) Champoux, J. J. (2001) DNA topoisomerases: Structure, function, and mechanism. *Annu. Rev. Biochem. 70*, 369−413.
(44) Pouliot, J. J., Robertson, C. A., and Nash, H. A. (2001) Pathways for repair of topoisomerase I covalent complexes in *Saccharomyces cerevisiae*. *Genes Cells 6*, 677−687.
(45) Liu, C. Y., Pouliot, J. J., and Nash, H. A. (2002) Repair of topoisomerase I covalent complexes in the absence of the tyrosyl-DNA phosphodiesterase Tdp1. *Proc. Natl. Acad. Sci. U.S.A. 99*, 14970−14975.
(46) Liu, C. Y., Pouliot, J. J., and Nash, H. A. (2004) The role of Tdp1 from budding yeast in the repair of DNA damage. *DNA Repair 3*, 593−601.
(47) Davies, D. R., Interthal, H., Champoux, J. J., and Hol, W. G. J. (2002) Insights into substrate binding and catalytic mechanism of human tyrosyl-DNA phosphodiesterase (Tdp1) from vanadate and tungstate-inhibited structures. *J. Mol. Biol. 324*, 917−932.
(48) He, X. P., van Waardenburg, R. C. A. M., Babaoglu, K., Price, A. C., Nitiss, K. C., Nitiss, J. L., Bjornsti, M. A., and White, S. W. (2007) Mutation of a conserved active site residue converts tyrosyl-DNA phosphodiesterase I into a DNA topoisomerase I-dependent poison. *J. Mol. Biol. 372*, 1070−1081.
(49) Tsao, Y. P., Russo, A., Nyamuswa, G., Silber, R., and Liu, L. F. (1993) Interaction between Replication Forks and Topoisomerase-I-DNA Cleavable Complexes: Studies in a Cell-Free Sv40 DNA-Replication System. *Cancer Res. 53*, 5908−5914.
(50) Takashima, H., Boerkoel, C. F., John, J., Saifi, G. M., Salih, M. A. M., Armstrong, D., Mao, Y., Quiocho, F. A., Roa, B. B., Nakagawa, M., Stockton, D. W., and Lupski, J. R. (2002) Tdp1 mutations cause autosomal recessive spinocerebellar ataxia with axonal neuropathy and further illuminate the pathway for topoisomerase I dependent DNA damage repair. *Am. J. Hum. Genet. 71*, 538−538.
(51) Takashima, H., Boerkoel, C. F., John, J., Saifi, G. M., Salih, M. A. M., Armstrong, D., Mao, Y. X., Quiocho, F. A., Roa, B. B., Nakagawa, M., Stockton, D. W., and Lupski, J. R. (2002) Mutation of Tdp1, encoding a topoisomerase I-dependent DNA damage repair enzyme, in spinocerebellar ataxia with axonal neuropathy. *Nat. Genet. 32*, 267−272.
(52) El-Khamisy, S. F., and Caldecott, K. W. (2006) TDP1-dependent DNA single-strand break repair and neurodegeneration. *Mutagenesis 21*, 219−224.
(53) El-Khamisy, S. F., Saifi, G. M., Weinfeld, M., Johansson, F., Helleday, T., Lupski, J. R., and Caldecott, K. W. (2005) Defective DNA single-strand break repair in spinocerebellar ataxia with axonal neuropathy-1. *Nature 434*, 108−113.
(54) Katyal, S., El-Khamisy, S. F., Russell, H. R., Li, Y., Ju, L., Caldecott, K. W., and McKinnon, P. J. (2007) Tdp1 facilitates chromosomal single-strand break repair in neurons and is neuroprotective in vivo. *EMBO J. 26*, 4720−4731.
(55) Griffin, J. L., Bowler, M. W., Baxter, N. J., Leigh, K. N., Dannatt, H. R. W., Hounslow, A. M., Blackburn, G. M., Webster, C. E., Cliff, M. J., and Waltho, J. P. (2012) Near attack conformers dominate β-phosphoglucomutase complexes where geometry and charge distribution reflect those of substrate. *Proc. Natl. Acad. Sci. U.S.A. 109*, 6910−6915.
(56) Dapprich, S., Komaromi, I., Byun, K. S., Morokuma, K., and Frisch, M. J. (1999) A new ONIOM implementation in Gaussian98. Part I. The calculation of energies, gradients, vibrational frequencies and electric field derivatives. *J. Mol. Struct.: THEOCHEM 461*, 1−21.
(57) Siegbahn, P. E. M., Tye, J. W., and Hall, M. B. (2007) Computational Studies of [NiFe] and [FeFe] Hydrogenases. *Chem. Rev. 107*, 4414−4435.
(58) Zampella, G., Kravitz, J. Y., Webster, C. E., Fantucci, P., Hall, M. B., Carlson, H. A., Pecoraro, V. L., and De Gioia, L. (2004) Quantum mechanical models of the resting state of the vanadium-dependent haloperoxidase. *Inorg. Chem. 43*, 4127−4136.
(59) Himo, F., and Siegbahn, P. E. M. (2003) Quantum chemical studies of radical-containing enzymes. *Chem. Rev. 103*, 2421−2456.
(60) Siegbahn, P. E. M., and Borowski, T. (2011) Comparison of QM-only and QM/MM models for the mechanism of tyrosinase. *Faraday Discuss. 148*, 109−117.
(61) Siegbahn, P. E. M., and Himo, F. (2009) Recent developments of the quantum chemical cluster approach for modeling enzyme reactions. *J. Biol. Inorg. Chem. 14*, 643−651.
(62) Siegbahn, P. E. M., and Himo, F. (2011) The quantum chemical cluster approach for modeling enzyme reactions. *Wiley Interdiscip. Rev.: Comput. Mol. Sci. 1*, 323−336.
(63) Blomberg, M. R. A., Borowski, T., Himo, F., Liao, R. Z., and Siegbahn, P. E. M. (2014) Quantum Chemical Studies of Mechanisms for Metalloenzymes. *Chem. Rev. 114*, 3601−3658.
(64) Leiros, I., McSweeney, S., and Hough, E. (2004) The reaction mechanism of phospholipase D from *Streptomyces* sp strain PMF. Snapshots along the reaction pathway reveal a pentacoordinate reaction intermediate and an unexpected final product. *J. Mol. Biol. 339*, 805−820.
(65) Leiros, I., Secundo, F., Zambonelli, C., Servi, S., and Hough, E. (2000) The first crystal structure of a phospholipase D. *Struct. Folding Des. 8*, 655−667.
(66) Davies, D. R., Interthal, H., Champoux, J. J., and Hol, W. G. J. (2002) The crystal structure of human tyrosyl-DNA phosphodiesterase, Tdp1. *Structure 10*, 237−248.
(67) Davies, D. R., Interthal, H., Champoux, J. J., and Hol, W. G. J. (2003) Crystal structure of a transition state mimic for Tdp1 assembled from vanadate, DNA, and a topoisomerase I-derived peptide. *Chem. Biol. 10*, 139−147.
(68) Interthal, H., Pouliott, J. J., and Champoux, J. J. (2001) The tyrosyl-DNA phosphodiesterase Tdp1 is a member of the phospholipase D superfamily. *Proc. Natl. Acad. Sci. U.S.A. 98*, 12009−12014.
(69) Raymond, A. C., Staker, B. L., and Burgin, A. B. (2005) Substrate specificity of tyrosyl-DNA phosphodiesterase I (Tdp1). *J. Biol. Chem. 280*, 22029−22035.
(70) Davies, D. R., Interthal, H., Champoux, J. J., and Hol, W. G. J. (2004) Explorations of peptide and oligonucleotide binding sites of tyrosyl-DNA phosphodiesterase using vanadate complexes. *J. Med. Chem. 47*, 829−837.
(71) Interthal, H., Chen, H. J., and Champoux, J. J. (2005) Human Tdp1 cleaves a broad spectrum of substrates, including phosphoamide linkages. *J. Biol. Chem. 280*, 36518−36528.
(72) Selvy, P. E., Lavieri, R. R., Lindsley, C. W., and Brown, H. A. (2011) Phospholipase D: Enzymology, Functionality, and Chemical Modulation. *Chem. Rev. 111*, 6064−6119.
(73) Gajewski, S., Comeaux, E. Q., Jafari, N., Bharatham, N., Bashford, D., White, S. W., and van Waardenburg, R. C. A. M. (2012) Analysis of the Active-Site Mechanism of Tyrosyl-DNA Phosphodiesterase I: A Member of the Phospholipase D Superfamily. *J. Mol. Biol. 415*, 741−758.
(74) Gajewski, S., Comeaux, E. Q., Jafari, N., Bharatham, N., Bashford, D., White, S. W., and van Waardenburg, R. C. A. M. (2012) Analysis of the Active-Site Mechanism of Tyrosyl-DNA Phosphodiesterase I: A Member of the Phospholipase D Superfamily (vol 415, pg 741, 2012). *J. Mol. Biol. 416*, 725.
(75) Frisch, M. J., Trucks, G. W., Schlegel, H. B., et al. (2009) *GAUSSIAN 09*, revision C.01, Gaussian, Inc., Wallingford, CT.
(76) Becke, A. D. (1993) Density-Functional Thermochemistry. 3. The Role of Exact Exchange. *J. Chem. Phys. 98*, 5648−5652.

DOI: 10.1021/acs.biochem.5b00396
Biochemistry 2015, 54, 4236−4247

(77) Lee, C. T., Yang, W. T., and Parr, R. G. (1988) Development of the Colle-Salvetti Correlation-Energy Formula into a Functional of the Electron-Density. *Phys. Rev. B 37*, 785−789.
(78) Petersson, G. A., and Al-Laham, M. A. (1991) A Complete Basis Set Model Chemistry. 2. Open-Shell Systems and the Total Energies of the 1st-Row Atoms. *J. Chem. Phys. 94*, 6081−6090.
(79) Hariharan, P. C., and Pople, J. A. (1973) Influence of Polarization Functions on Molecular-Orbital Hydrogenation Energies. *Theor. Chim. Acta 28*, 213−222.
(80) Foresman, J. B., and Frisch, Æ. (1993) *Exploring Chemistry with Electronic Structure Methods*, 2nd ed., p 110, Gaussian, Inc., Pittsburgh, PA.
(81) Hay, P. J., and Wadt, W. R. (1985) Ab initio Effective Core Potentials for Molecular Calculations: Potentials for the Transition-Metal Atoms Sc to Hg. *J. Chem. Phys. 82*, 270−283.
(82) Hay, P. J., and Wadt, W. R. (1985) Ab initio Effective Core Potentials for Molecular Calculations: Potentials for K to Au Including the Outermost Core Orbitals. *J. Chem. Phys. 82*, 299−310.
(83) Word, J. M., Lovell, S. C., Richardson, J. S., and Richardson, D. C. (1999) Asparagine and glutamine: Using hydrogen atom contacts in the choice of side-chain amide orientation. *J. Mol. Biol. 285*, 1735−1747.
(84) Word, J. M., Lovell, S. C., LaBean, T. H., Taylor, H. C., Zalis, M. E., Presley, B. K., Richardson, J. S., and Richardson, D. C. (1999) Visualizing and quantifying molecular goodness-of-fit: Small-probe contact dots with explicit hydrogen atoms. *J. Mol. Biol. 285*, 1711−1733.
(85) Doncheva, N. T., Klein, K., Domingues, F. S., and Albrecht, M. (2011) Analyzing and visualizing residue networks of protein structures. *Trends Biochem. Sci. 36*, 179−182.
(86) Doncheva, N. T., Assenov, Y., Domingues, F. S., and Albrecht, M. (2012) Topological analysis and interactive visualization of biological networks and protein structures. *Nat. Protoc. 7*, 670−685.
(87) DeYonker, N. J., Kelso, D. K., III, Webster, C. E., and Homayouni, R., manuscript in preparation.
(88) Comeaux, E. Q., Cuya, S. M., Kojima, K., Jafari, N., Wanzeck, K. C., Mobley, J. A., Bjornsti, M.-A., and van Waardenburg, R. C. A. M. (2015) Tyrosyl-DNA Phosphodiesterase I Catalytic Mutants Reveal an Alternative Nucleophile That Can Catalyze Substrate Cleavage. *J. Biol. Chem. 290*, 6203−6214.

DOI: 10.1021/acs.biochem.5b00396
Biochemistry 2015, 54, 4236−4247